

Cosmic-Ray Acceleration by Forward and Reverse Shocks in Young Supernova Remnants

MARTIN POHL^{1,2}, VIKRAM DWARKADAS³, IGOR TELEZHINSKY²

¹Universität Potsdam, Institut für Physik & Astronomie, Karl-Liebknecht-Strasse 24/25, 14476 Potsdam, Germany

²DESY, Platanenallee 6, 15738 Zeuthen, Germany

³University of Chicago, Department of Astronomy & Astrophysics, 5640 S Ellis Ave, AAC 010c, Chicago, IL 60637, U.S.A.

pohlmadq@gmail.com

DOI: 10.7529/ICRC2011/V06/0137

Abstract: Observations of soft gamma-ray spectra from shell-type Supernova Remnants (SNRs) are not in line with standard Non-linear Diffusive Shock Acceleration (NDSA). We explore alternative ways to explain the observations by means of test-particle DSA. The main novelty is the investigation of the impact of the reverse shock in young SNRs using 1-D simulations of the hydrodynamical evolution and different magnetic field profiles in the shocked material of the SNR. We study the temporal evolution of non-thermal particle distributions and their radiation in a broad domain of energies. We synthesize the surface brightness maps and explore the evolution of their brightness profiles. It is demonstrated that the reverse shock significantly contributes to the cosmic ray particle population of the SNRs, strongly modifying the spatial distribution of particles and noticeably affecting the volume-integrated particle spectra. Therefore, the spectrum and morphology of emission, and their time evolution, are drastically different from a pure forward-shock solutions. In some of our models we observed rather soft high-energy gamma-ray spectra, which are well in agreement with current observations of Cherenkov telescopes.

Keywords: cosmic rays, supernova remnants

1 Introduction

Diffusive shock acceleration (DSA) at SNR shocks [1, 2, 3, 4] is thought to be the most likely mechanism that can accelerate CRs up to 10^{15} eV, [5]. CRs can modify the shock structure by decelerating the incoming plasma in the precursor region (see [6] for a review and references therein). Observationally, it is unclear whether or not the CR-acceleration efficiency is sufficiently high for a significant feedback [7, 8], but if so, SNR shocks may become modified, and the particle spectra in nonlinear DSA (or NDSA) become soft ($s > 2$, $N(E) \propto E^{-s}$) at low energy and hard ($s < 2$) at high energy. Recent γ -ray observations of shell-type SNRs tend to show soft spectra ($\Gamma > 2$, $N_\gamma(E) \propto E^{-\Gamma}$): RX J1713.7-3946 [9, 10], RX J0852.0-4622 [11], RCW 86 [12], SN 1006 [13], Cas A [14, 15], IC 443 [16, 17] and other [18, 19, 20]. Assuming the radiation was produced by hadrons, the particle spectra would be softer than predicted by NDSA.

We investigate the diversity of particle spectra that can be produced by shocks of young SNRs in a test-particle mode, concentrating for simplicity on type-I SN in this paper. We consider acceleration by both forward and reverse shocks. As was noted earlier [21], not only the forward shock (FS) but also the reverse shock (RS) may produce high-energy particles or re-accelerate the particles produced by the FS [22]. We investigate the influence of several assumptions

on radial dependencies of MF inside SNRs and explore how Alfvénic drift may affect the total particle spectra in SNR. Besides calculating the total particle spectra, we provide intensity profiles in the radio band, X rays and γ rays.

2 Cosmic-Ray Acceleration

A test-particle description is applicable if the CR pressure at the shock is less than 10% of the shock ram pressure [23]. Therefore, if one limits the amount of energy contained in CRs and the CR pressure at the shock, the acceleration can be treated by independently solving the cosmic-ray transport equation and the hydrodynamic equations of SNR evolution. The cosmic-ray transport equation is a diffusion-advection equation in both space and momentum [24]:

$$\frac{\partial N}{\partial t} = \nabla(D_r \nabla N - \vec{v} N) + \frac{\partial}{\partial p} \left(p^2 D_p \frac{\partial N}{\partial p} \right) - \frac{\partial}{\partial p} \left((N \dot{p}) - \frac{\nabla \vec{v}}{3} N p \right) + Q \quad (1)$$

where N is the differential number density of cosmic rays, D_r is the spatial diffusion coefficient, \vec{v} the advective velocity given by a 1-D hydrodynamical simulation, \dot{p} are the energy losses, D_p is the momentum-space diffusion coefficient ignored in this paper, and Q is the source term representing the injection of the thermal particles into the acceleration process given as

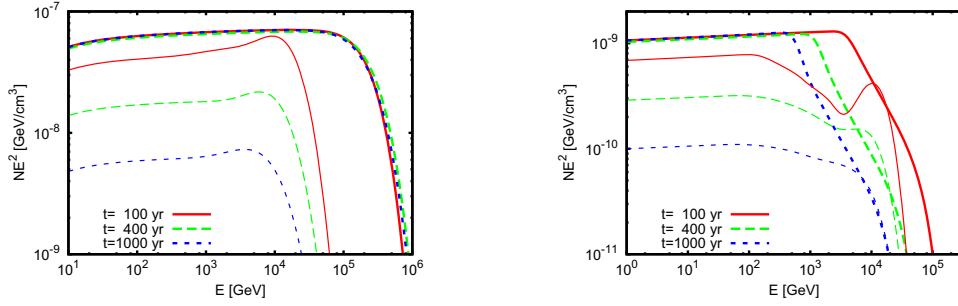


Figure 1: The FS (thick lines) vs. the RS (thin lines) contributions to the spectra of protons (left) and electrons (right) for different SNR ages.

$$Q = \eta_i n_u |V_{sh} - v_u| \delta(r - R_{sh}) \delta(p - p_{inj}), \quad (2)$$

where η_i is the injection efficiency parameter, n_u is the number density of plasma in the shock upstream region, V_{sh} is the shock speed, v_u is the plasma velocity in the shock upstream region, r is the distance from the SNR center, R_{sh} is the radius of the shock, p is the particle momentum, and p_{inj} is the momentum of the injected particles. In the current paper we assume spherical symmetry and do not consider the momentum-diffusion term representing stochastic (second order Fermi) acceleration.

We normalize the spatial coordinate in Eq. 1 to the shock radius, introducing coordinate $x = r/R_{sh}$, and then substitute the coordinate x with a new coordinate, x_* , for which we use a uniform grid when solving Eq. 1:

$$(x - 1) = (x_* - 1)^3 \quad (3)$$

These simple transformations allow us i) to place the shock at the center of a known cell at any given time and ii) to resolve the shock vicinity for low-energy particles with only a few hundred bins in the spatial coordinate, x_* . Then, Eq. 1 is solved in spherically-symmetric geometry using implicit finite-difference methods implemented in the *FiPy* [25] library modules. We make separate runs for the FS and the RS, using the appropriate coordinate transformations to obtain the highest resolution where injection occurs.

To study the evolution of the SNR shock waves over time, we have performed spherically-symmetric hydrodynamic simulations using the VH-1 code [26]. The simulations are based on an expanding grid [27, 28], which tracks the motion of the outer shock and expands along with it. Thus, a high resolution is maintained right from the start of the simulations, which is essential considering that the remnant size increases by about 6 orders of magnitude during the simulation. The expanding grid also has another advantage - the position of the forward shock is almost stationary on the grid over most of the evolution, which is useful in computing the particle spectrum. The simulation commences with a grid of size 6×10^{-5} pc. By the end of the simulation, which is carried on for about 1000 years, it has grown to more than 10 pc. The shocked ejecta reach a maximum density on the inner side of the contact discontinuity,

while the shocked ambient medium reaches a minimum on the outer side. The temperature therefore reaches a maximum at the CD for the shocked ambient medium. This distinguishes it from the structure obtained for a power-law profile expanding into the ambient medium, as would be more appropriate for a Type II or core-collapse SN [29].

Finally, the numerical solution of the hydrodynamic equations is mapped onto the spatial coordinate x_* (cf. Eq 3) in which we have written the particle transport equation (Eq. 1). The shocks, which are invariably smeared out in the hydrodynamic simulation, are re-sharpened by interpolation toward a point-like jump in density, flow velocity, and pressure. This is necessary to maintain a realistically fast acceleration at GeV-to-TeV energies.

The strength of the magnetic field in the SNR is one of the crucial parameters for CR acceleration, particularly so in the shock regions. Since we assume Bohm diffusion here, the MF determines the mean free path of the particle before it is scattered. The actual mechanisms of MF amplification are subject of ongoing research. Here we are interested in the impact of various MF profiles on the spectra of accelerated particles. Therefore, we introduce a set of simple models which describe the temporal and spatial evolution of the magnetic field in a SNR. In D models the MF scales with gas density, whereas in P models it follows the gas pressure. We assume two possible values of the MF at the SNR forward shock at $t_m = 500$ years, $B_{FS} = 75 \mu\text{G}$ and $B_{FS} = 300 \mu\text{G}$. These values are taken in accordance with average limits given by the observational data on the MF for young SNRs such as Tycho [30].

3 Results and Discussion

In all models without Alfvénic drift, the particles accelerated at the FS obey the classical power-law spectrum with index $s \simeq 2$ up to the energy, at which the escape of the system or energy losses inhibit further acceleration. As predicted by DSA, for protons $E_{max,p} \sim V_{sh}^2 B_0 t$. The ability of the RS to accelerate particles depends on the MF configuration at the location of the RS. With the MF profiles assumed here, the RS is capable of accelerating particles to sufficiently high energies and intensities to

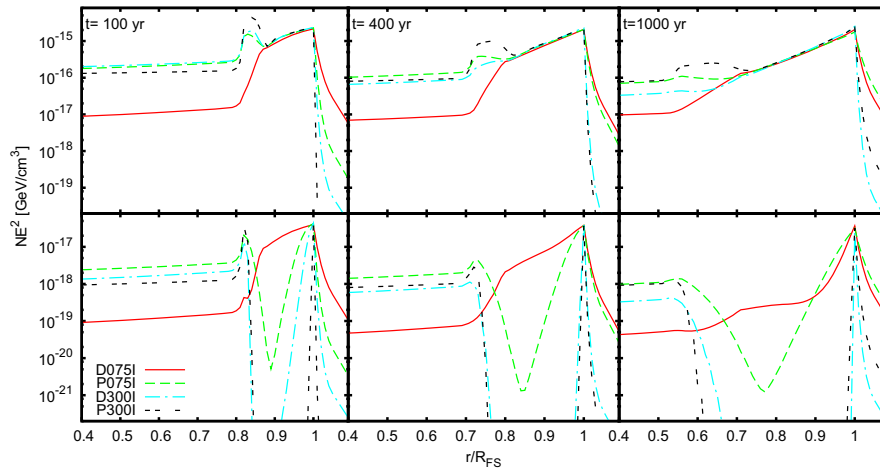


Figure 2: The time evolution of the spatial distribution of protons (top row) and electrons (bottom row) at energy of 20 TeV

contribute to the total volume-integrated particle spectra of the SNR. In the absence of Alfvénic drift, the RS spectra show slopes similar to those at the FS, with the exception of some hardening at higher energies and a bump near E_{max} (see Figure 1).

The MF profiles in the SNR interior affect the radial distribution of CRs and their subsequent emission, especially so for leptons. In Fig.2 we plot the evolution of the radial distribution of protons and electrons at the energy of 20 TeV, which could be a characteristic energy of the particles producing high-energy emission. One can clearly see that electrons suffer significant losses in the shocked region where the MF is high. The number density of protons falls nearly exponentially from the FS towards the CD. There is a noticeable peak in the CR distributions near the RS. Whereas electrons peak exactly at the RS, protons are accumulated between the RS and the CD. At 100 years, the CR number density close to the RS is even higher than at the FS. At 400 years the peak is still clearly visible, however already at 1000 years only a minor bump is observed. In the ejecta region, where the MF is low, both particle species show nearly uniform distributions. To permit morphological studies of SNR at different ages, we computed radial intensity profiles at characteristic wavebands (radio @1.4 GHz, X-rays @3 keV, gamma-rays @1 TeV). In Fig. 3 we plot normalized intensity profiles separately for leptonic and hadronic emission.

It is astonishing to see how the brightness profiles change with time. At 100 years both shocks are bright and visible in all bands except for the FS in radio waves, which are emitted by low-energy electrons. The contribution of the RS to the total emission is high at this time. The low-energy electrons cannot propagate far from their point of origin, and therefore the relatively high injection rate at the RS in the early phase renders it much brighter than the FS in radio band. Pion-decay gamma rays are copiously produced in the ejecta region on account of the high tar-

get density there. At 400 years the contribution of the RS region becomes less prominent, but is still visible. Only in synchrotron X-rays (and IC in D075I/A models) the RS becomes insignificant. The 3 keV synchrotron X-rays are created by electrons of rather high energy (~ 13.5 TeV for $B = 300 \mu\text{G}$ and ~ 27 TeV for $B = 75 \mu\text{G}$). At this age the RS is no longer able to boost electrons up to these energies. The electrons accelerated at the FS suffer from losses on their way to the SNR interior, and therefore the synchrotron emission becomes noticeably filamentary, especially in high-MF models. In the models with high MF, a plateau of high-intensity IC emission appears in the ejecta region. Between the two shocks, high-energy electrons are few on account of severe energy losses, so the IC emission is suppressed. At the same time, the electrons that propagated into the ejecta region, where the MF is low, accumulate there and account for the bright IC emission. This trend continues with age, and after 1000 years we observe a bright plateau of IC emission from the SNR center, while the FS appears very filamentary. There is almost no trace of emission from the RS after 1000 years in the other wavebands. X-ray synchrotron emission is seen as a thin filament near the FS, especially in the models with high MF.

4 Conclusions

We have studied particle acceleration by both forward and reverse shocks in young Type-Ia SNR, using gas-flow profiles derived from 1-D hydrodynamical simulations to solve the cosmic-ray transport equation in test-particle approach. It is important to account for the contribution of the RS to cosmic-ray particle population in the initial 400 - 600 years of SNR evolution, depending on the density of the ambient medium and the magnetic-field profile. At that time the RS is able to accelerate particles up to very high energies, and the number of accelerated particles is comparable to that at the FS. This is well visible in volume-integrated parti-

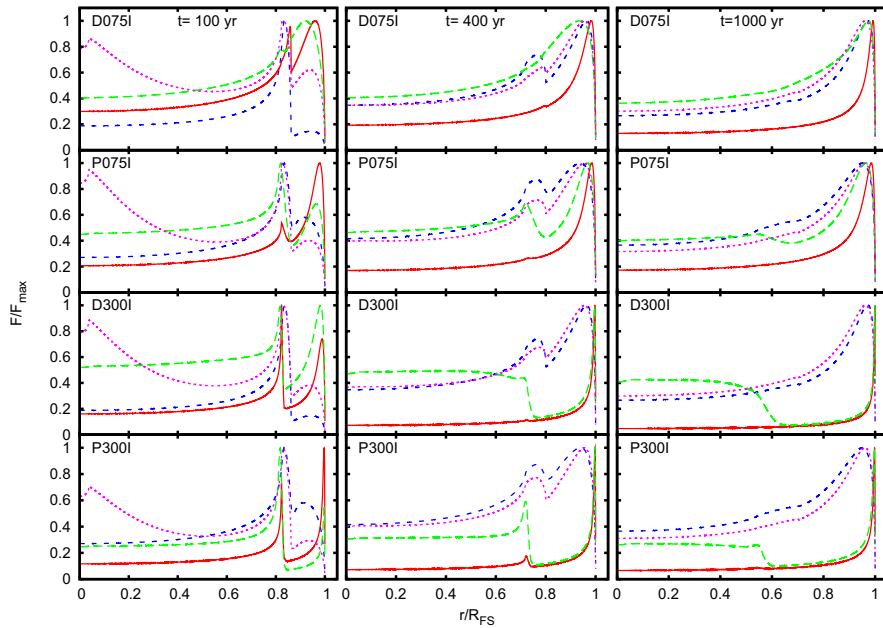


Figure 3: The radial intensity profiles of the SNR in different models at different wavelength and ages. Radio @1.4 GHz (short-dashed blue), X-rays @3 keV (solid red), IC @1 TeV (long-dashed green), pion-decay @1 TeV (dotted pink).

cle spectra, the distribution of high-energy particles in the SNR, as well as in the morphology of particle radiation. The significance of the RS contribution falls with time, and although it is still visible in particle spectra up to 1000 years or so, it is barely noticeable in the emission spectra and morphology.

We found that the total volume-integrated particle spectra of the SNR differ from single-shock test-particle solutions, especially for very young SNRs. The choice of MF profiles affected the relative contribution to the total spectrum of the RS and the FS. Additionally, Alfvénic drift of scattering centers in the shock precursors gives rise to additional spectral feature, whose appearance and time evolution depends on the choice of MF profile. Interesting is that some of the spectra (both electron and protons) exhibit features typical of NDSA, such as spectral concavity and high-energy bumps. One difference is that our test-particle spectra are softer than those of NDSA, which may provide a better agreement with γ -ray spectra observed from SNRs.

References

- [1] W. I. Axford, E. Leer, G. Skadron, in: XI. International Cosmic Ray Conference, 1977, 132–137.
- [2] G. F. Krymskii, Akademiia Nauk SSSR Doklady, 1977, **234**, 1306–1308.
- [3] A. R. Bell, MNRAS, 1978, **182**, 147–156.
- [4] R. D. Blandford, J. P. Ostriker, ApJL, 1978, **221**, L29–L32.
- [5] P. O. Lagage, C. J. Cesarsky, A&A, 1983, **125**, 249–257.
- [6] M. A. Malkov, L. O’C Drury, Rep. Progr. Phys., 2001, **64**, 429–481.
- [7] J. S. Warren, et al., ApJ, 2005, **634**, 376–389.
- [8] J. C. Raymond, J. Vink, E. A. Helder, A. de Laat, ArXiv:1103.3211.
- [9] F. A. Aharonian, et al. Nature, 2004, **432**, 75–77.
- [10] F. Aharonian, et al., A&A, 2007, **464**, 235–243.
- [11] F. Aharonian, et al., ApJ, 2007, **661**, 236–249.
- [12] F. Aharonian, et al., ApJ, 2009, **692**, 1500–1505.
- [13] F. Acero, et al. A&A, 2010, **516**, A62+.
- [14] V. A. Acciari, et al., ApJ, 2010, **714**, 163–169.
- [15] A. A. Abdo, et al., ApJL, 2010, **710**, L92–L97.
- [16] V. A. Acciari, et al., ApJL, 2009, **698**, L133–L137.
- [17] A. A. Abdo, et al., ApJ, 2010, **712**, 459–468.
- [18] D. Castro, P. Slane, ApJ, 2010, **717**, 372–378.
- [19] A. A. Abdo, et al., Science, 2010, **327**, 1103–.
- [20] A. A. Abdo, et al., ApJ, 2010, **718**, 348–356.
- [21] V. N. Zirakashvili, F. A. Aharonian, ApJ, 2010, **708**, 965–980.
- [22] K. M. Schure, A. Achterberg, R. Keppens, J. Vink, MNRAS, 2010, **406**, 2633–2649.
- [23] H. Kang, D. Ryu, ApJ, 2010, **721**, 886–892.
- [24] J. Skilling, MNRAS, 1975, **172**, 557–566.
- [25] J. E. Guyer, D. Wheeler, J. A. Warren, Computing in Science and Engineering, 2009, **11**, 6–15.
- [26] J. M. Blondin, P. Lundqvist, ApJ, 1993, **405**, 337–352.
- [27] V. V. Dwarkadas, ApJ, 2005, **630**, 892–910.
- [28] V. V. Dwarkadas, ApJ, 2007, **667**, 226–247.
- [29] V. V. Dwarkadas, R. A. Chevalier, ApJ, 1998, **497**, 807–.
- [30] Acciari, V. A., et al., ApJL, 2011, **730**, L20